

1 **Evaluation of AMSR-E Sea Ice Temperature product: Comparison with Antarctic**
2 **IMB Buoy Data**

3 M. J. Lewis^{1,2}, H. Xie², and S. F. Ackley²

4
5 ¹Southwest Research Institute, San Antonio, TX

6 ²Laboratory for Remote Sensing and Geoinformatics, University of Texas at San Antonio

7 San Antonio, TX, USA

8
9 **Abstract**

10
11
12 **1. Introduction**

13 Antarctic sea ice plays an important and complex role in the climate system, regulating
14 heat and energy transfer, gas exchange, and many seasonal and cyclic environmental patterns
15 that affect the global system. The formation and decay of Antarctic sea ice annually represents a
16 significant energy transfer and phase transformation, cycling from a summer minimum of about
17 3 million square kilometers of ocean area coverage to a winter maximum of about 19 million
18 square kilometers. In addition to climatic importance, the sea ice pack itself provides a rich
19 environment for marine life (from large mammals to microbes) that exist in polar ecosystems.
20 Sea ice temperature is an important physical parameter that not only affects sea ice properties
21 such as salinity, thermal conductivity, and porous microstructure [Golden, et al. 2001; Weeks
22 and Ackley, 1986], but also affects sea ice biomes and productivity [Ackley, et al., 2006], carbon
23 dioxide gas exchange between the ocean and atmosphere [De Lille, et al., *], and the production

24 dimethyl sulfide (DMS) and dimethylsulfoniopropionate (DMSP) in sea ice as precursors to
25 atmospheric sulfate aerosols [Brabant, et al., 2008]. The ability to remotely derive sea ice
26 temperature from space has significant importance, not only in the advancement of remote
27 sensing applications of satellite data, but also in the context of understanding and modeling
28 physical interactions of sea ice with biological and climate systems. The Integrated Global
29 Observing Strategy (IGOS), a strategic planning process implemented by fourteen international
30 scientific organizations, has identified “data fusion” remote sensing products as a critical long-
31 term goal of cryospheric monitoring programs, with specific emphasis in the near-term on
32 developing and validating satellite products during the International Polar Year [IGOS, 2007].

33 Passive microwave remote sensing products are particularly useful in the study of polar
34 regions due to their long-term (~30-year) record of observations and that passive microwave
35 emissions from the Earth do not rely on solar illumination for retrievals during the long periods
36 of polar darkness [Parkinson, 2004; Comiso, et al., 2008]. A number of different algorithms have
37 been developed for application to polar (snow and ice) environments and principally rely on the
38 high contrast in emissivity between snow, ice and ocean water at many microwave frequencies in
39 the electromagnetic spectrum. Previous studies by the authors have documented inconsistencies
40 in physical characteristics between the Advanced Microwave Scanning Radiometer- Earth
41 Observing System (AMSR-E) Sea Ice Temperature product and Antarctic field data obtained
42 from a number of different locations at differing time periods [Lewis and Xie, 2006; Lewis, et
43 al., 2006]. These studies indicated that the AMSR-E Sea Ice Temperature product yielded ice
44 interface temperatures that were colder, rather than warmer beneath areas of maximum snow
45 cover and that unrealistically low ice interface temperatures (as compared with the range of field
46 data) observed in the austral spring and summer season. It was postulated that the AMSR-E sea

47 ice temperature anomalies resulted from reduced emissivity at the snow/ice interface due to sea
48 water flooding. However, none of the specific field data examined from Antarctic field studies
49 was temporally coincident with AMSR-E satellite coverage. This limitation precluded any
50 conclusion or specific validation other than the general observations stated above. In particular,
51 the current evaluation attempts to overcome this limitation by comparison of spatially and
52 temporally co-incident in situ sea ice temperature data from two Antarctic field programs with
53 remotely sensed AMSR-E values.

54 **2. AMSR-E Sea Ice Temperature Product**

55 The AMSR-E sensor provides multi-band passive microwave measurements of the Earth
56 with twice daily coverage. The Sea Ice Temperature (L3, 25 km) data product obtained from the
57 National Snow and Ice Data Center (NSIDC) is derived principally from the brightness
58 temperature of passive microwave emissions at 6.9 GHz frequency using the AMSR Bootstrap
59 Algorithm (ABA) [Comiso, et al., 2003]. The effects of atmospheric interactions and surface
60 scattering are reported to be minimized at this frequency and the contrast between sea ice and
61 open water is high, however, the spatial resolution is greatly reduced to 25 km [Cavalieri and
62 Comiso, 2000, Comiso et al., 2008]. The ABA incorporates a technique using the average
63 brightness temperature (T_B) from 6.9V and 37V frequency bands to estimate the initial ice
64 concentration (C_i) using a linear mixing equation. The initial estimate of C_i is utilized to
65 calculate the effective emissivity (ϵ_B) using the reference emissivities for ice (ϵ_i) and open water
66 (ϵ_o) and the mixed pixel equation:

$$67 \quad \epsilon_B = \epsilon_i C_i + \epsilon_o (1 - C_i) \quad (\text{Eqn. 1})$$

68 The initial ice concentration is calculated from reference emissivities corresponding to
69 ice and ocean end member tie points. The temporal and spatial variability of reference

70 emissivities may be attributed to varying ice type, changes in snow cover, and wind roughening
71 of open water which can lead to errors and inconsistencies in calculated ice concentrations
72 [Andersen, et al., 2006, Comiso and Parkinson, 2008]. The open water tie points of the ABA
73 algorithm are set close to the minimum brightness temperature to minimize the influence of
74 atmospheric effects. This has been reported to lead to a positive bias in sea ice concentration
75 retrieved over open water resulting in low sea ice concentrations [Andersen, et al., 2006].

76 The kinetic (physical) temperature (T_p) of the sea ice/snow interface is subsequently
77 computed using the following equation where T_B (6.9V) is the brightness temperature measured
78 from the 6.9 GHz vertically polarized band.

$$79 \quad T_p = T_B (6.9V) / \epsilon_B (6.9V) \quad (\text{Eqn. 2})$$

80 The reference emissivities for 19V and 37V channels are subsequently computed using T_p and T_B
81 for each respective channel and the final ice concentration (C_I) is then computed using these
82 channels and the ABA algorithm. The new ice concentration is then used to calculate sea ice
83 interface temperature (T_s) in Equation 3, where T_o the ocean temperature is set equal to 271° K.

$$84 \quad T_s = [T_p - T_o (1-C_I)] / C_I \quad (\text{Eqn. 3})$$

85 It was reported [Comiso, pers. com.] that the ice concentration algorithm used to compute the
86 Sea Ice Temperature product was changed in mid 2005 to the NASA Team algorithm- version 2
87 (NT2). The algorithm substitution was shown to result in a significant change in an overall
88 distribution of sea ice temperature (2005) calculated on a circum-polar basis for Antarctic,
89 tending toward much lower values [Lewis et al., 2006].

90 For this paper, the time series of AMSR-E daily averaged Sea Ice Temperature, Ice
91 Concentration, and T_B from 6.9, 10.7, 18.7, 23.8, 36.5, and 89.0 GHz vertically and horizontally
92 polarized channels were obtained from the NSIDC for the time period corresponding the

93 operation of the two Antarctic IMB experiments in 2002 and 2007. The original AMSR-E files in
94 HDF format were converted to GeoTIFF images using the MODIS Reprojection Tool (MRT)
95 application to allow their import and georeferencing in ArcMap GIS software. Buoy position
96 data (latitude, longitude, and time) were also imported into ArcMap and saved in ESRI shapefile
97 format so that the positions could be projected to south pole stereographic coordinates and
98 converted to ArcInfo coverage. An Arc Macro Language (AML) script developed at UTSA was
99 utilized to run in an ArcInfo shell that transfers the GeoTIFF to grid (raster) dataset, and outputs
100 a spatially weighted value of the grid cell according to the coverage (buoy position). The AML
101 script uses the “lattice spot” routine in ArcInfo to provide spatial-weighted values based on bi-
102 linear interpolation of the four nearest pixel values. The resulting data set includes cell grid
103 values of each parameter (sea ice temp, ice concentration, etc) for each buoy position at different
104 times as represented by the daily AMSR-E image.

105 An example of daily buoy position data superimposed upon a 25 km AMSR-E grid is
106 given in *Figure 1*. Each colored segment represents multiple buoy drift positions corresponding
107 to a single day and therefore a single Daily AMSR-E image. All colored segments together show
108 the total cumulative drift of the buoy during the period of operation. The time series of AMSR-E
109 data was extracted to be both spatially and temporally coincident with the in situ temperature
110 data, however the resolution of the AMSR-E grid is very coarse in comparison to “point” in situ
111 temperature data. The interpretation of AMSR-E ice temperatures is therefore complicated by the
112 presence of different ice types and thickness, varying snow cover which provides thermal
113 insulation, and areas of sea water flooding at the snow/ice interface, thereby representing a
114 spatial average over the 25 km by 25 km pixel size. For further evaluation of the validity of the

115 AMSR-E product, it is essential to have a suitable characterization of the spatial variability of
116 snow and ice conditions present within the pixel area.

117 **3. Sea Ice Temperature data from SOGLOBEC**

118 In situ ice temperature data from two Antarctic programs were utilized for comparison
119 with AMSR-E Sea Ice Temperature data. The first data set included in situ data generated from
120 an IMB designed and constructed by the Cold Regions Research and Engineering Lab (CRREL)
121 that was installed during the Southern Ocean Global Ecosystems Dynamics (SOGLOBEC)
122 experiment in the Marguerite Bay area on the west side of the Antarctic peninsula [Perovich et
123 al., 2004]. The buoy was equipped with GPS tracking for position, ultrasonic distance meter for
124 snow surface elevation, upward looking sonar for under ice elevation, air temperature sensor,
125 barometric pressure sensor, and a string of temperature sensors (thermistors) extending from the
126 air above the snow pack through snow, ice and ocean water at 5 centimeter spacing. Data
127 collected by the buoy's acquisition system, typically on a 2 hour interval, was transmitted
128 periodically by ARGOS satellite link to CRREL. The air, snow, and ice temperatures obtained
129 from IMB 07948-02, operational from September 3 to December 5, 2002 at time periods co-
130 incident with AMSR-E coverage, were used in this evaluation. The IMB buoy drifted within an
131 area from approximately 68.5° W to 70.5°W longitude and 65.3° S to 66.6° S latitude.

132 During the SOGLOBEC experiment, the sea ice floes were noted by Perovich, et al.
133 (2004) to have flooding of the snow-ice interface on a region-wide basis with negative freeboard
134 initially reported in approximately 20% of the measured floes. Data from this IMB buoy
135 indicates an ice floe with characteristic thickness slightly greater than 0.5 meters and a snow
136 cover varying from 25 cm initially to over 40 cm by the end of operation. Assuming typical snow
137 and ice densities, this floe would be expected to have approximately neutral freeboard at the

138 onset of IMB operation, which is also supported by the initial low ice interface temperature. The
139 time-series of upward directed sonar sensors on the buoy show ablation of ice mass beginning at
140 the end of October and continuing to the end of transmission in December. The thickness of
141 snow cover is variable, but shows an overall increasing trend, which indicates the potential for
142 flooding of the snow/ice interface due to isostatic balance. The time series of temperature data
143 indicate episodic flooding of the snow/ice interface and refreezing through the end of October,
144 after which the sea ice temperature remains fairly constant near the freezing temperature of sea
145 water, as shown in *Figure 2*. The AMSR-E Sea Ice Temperature product coincident in both
146 temporally and spatially is also plotted in Figure 2 for comparison. Missing AMSR-E data are
147 shown as a break in the line from September 12 to 20, 2002.

148 The temperature traces are referenced from the original position of the snow/ice interface
149 (0 cm) with height convention given in the snow pack as a positive distance above the original
150 snow/ice interface. The sea ice and snow temperatures begin to increase around September 7 in
151 response to an atmospheric warming trend that lasts about a week before the temperatures begin
152 to decline again in the snow pack at +10 cm. The ice interface floods with sea water at the +5 cm
153 level and tracks closely with the temperature of the original snow/ice interface (0 cm). The
154 flooded snow subsequently re-freezes and floods again in two additional events during October
155 before the temperature at +10 cm level stabilizes at the end of October. This timing coincides
156 with the start of ice ablation from the bottom of the floe. Of particular interest is the AMSR-E
157 sea ice temperature, which remains below the recorded ice temperature over the entire record. At
158 the occurrence of the interpreted flooding events, the in situ sea ice temperature increases,
159 however the AMSR-E temperature shows a corresponding drop of about 4 to 6 degrees. Beyond
160 the end of October, the AMSR-E sea ice temperature shows erratic swings even though recorded

161 air temperatures remain relatively stable near 0° C. As shown in *Figure 3*, the AMSR-E derived
162 ice concentration drops below 80% after the end of October indicating that the ice pack is losing
163 consistency.

164 **4. Sea Ice Temperature data from SIMBA**

165 The second data set from Antarctic field programs included three IMBs placed during the
166 Sea Ice Mass Balance in the Antarctic (SIMBA) program, also designed and constructed by
167 CRREL, that collected time series of sea ice temperature data in the Bellingshausen Sea of
168 Antarctica (approximately 90°W longitude and 70° S latitude) during the month of October
169 2007. A 27-day drift station was established on an approximately 2 km diameter sea ice floe of
170 mixed ice types, know as Belgica Station (after the historic Belgian expedition of 1897-1899 that
171 wintered-over in the area). Two of the buoys (at the Brussels Site) remained after the departure
172 of the NB Palmer and collected ice temperature data from October 2 to December 14, 2007 and
173 October 12 to December 6, 2007, respectively. The third IMB (at the Liege Site) was installed on
174 October 5, 2007 and removed before departure on October 23, 2007. In addition, temperature
175 data loggers (Onset Tidbit v2) were installed between October 16 and 22, 2007 in Snow Pit 2G
176 (at the Fabra Site) over heavily deformed thick ice that was extensively flooded at the snow/ice
177 interface.

178 The Belgica Station ice floe (SIMBA drift station) and surrounding area are best
179 characterized by ASPeCt ice observations [Worby and Allison, 1999] performed from the ship's
180 bridge during the transit into and out of the ice pack. The ice observations performed within the
181 4 hours prior to reaching Belgica Station (estimated 20 km) have been recorded as approximately
182 40% concentration of thick deformed ice (multi-year) with thick snow cover of 0.75 to 1 meter,
183 and approximately 60% concentration of first year ice with 10% or less weathered ridges and

184 thinner (20 to 50 cm) snow cover. Sea Ice categories with less than 10% concentration
185 represented are not recorded in the ice observations. For observations performed at Belgica
186 Station, young ice or nilas with no snow cover did not meet this threshold. A photograph
187 showing the mixture of ice types prevalent at Belgica Station is given in **Figure 4**. Extensive
188 snow cover on sea ice was observed throughout the region during the month long drift period.
189 The snow and ice environment is relevant in understanding the mixture of information contained
190 in a 25 km AMSR-E pixel of low spatial resolution when comparing to in situ “point”
191 information. Since low emissivity values representing open water or frazil ice are removed from
192 the AMSR-E data by linear unmixing equation in the algorithm, the range of sea ice interface
193 temperatures from AMSR-E are expected to be bounded by the ice types observed at the
194 Brussels and Fabra sites. The ice concentration obtained from AMSR-E data for the time period
195 covering the drift of Belgica Station is given in **Figure 5**. The concentration varies from a
196 minimum of 82% (October 8) to a maximum of 100%. The ice concentration remains above 95%
197 for the majority of the time period, except from the dates October 8 through October 13.

198 The Brussels Site contained relatively level 0.5 meter thick ice with thin snow cover of
199 approximately 7 cm mean thickness. Due to relatively thin snow cover at the Brussels Site, the
200 temperature of the ice interface more directly reflects colder air temperatures, and therefore
201 represents the cold end member of ice conditions present at Belgica Station. The Fabra Site
202 contained thicker deformed ice (~2 meters thick) with thick snow cover (mean 68 cm) and
203 extensively flooded interface. Due to thick insulating snow cover and presence of warmer sea
204 water at the interface, the Fabra Site represents the warm end member of ice conditions present
205 at Belgica Station. The Liege Site represents an intermediate ice condition with approximately 1
206 meter thick ice and 30 to 50 cm snow cover. Flooding of the snow/ice interface was observed at

207 the Liege Site. Representative profiles of the Fabra and Brussels sites are given in *Figure 6* and
 208 summary statistics from representative measurements obtained along the transect lines at both
 209 sites are given in Table 1.

210 Table 1 – Comparison of Summary Statistics for Fabra and Brussels Sites

Fabra Site (10/7/07)				n=602
Parameter	Mean	St Dev	Min	Max
Snow Depth (m)	0.677	0.313	0.070	1.900
Surface Elevation (m ASL)	0.675	0.289	0.079	1.539
S/I Interface (m ASL)	-0.002	0.248	-0.592	1.339
EM Ice Thickness (m)	1.733	0.693	0.437	3.674
*Measured Ice Thick (m)	2.328	1.251	0.600	5.010
*Measured Freeboard (m)	-0.027	0.143	-0.450	0.270

Brussels Site (10/3/07)				n=402
Parameter	Mean	St Dev	Min	Max
Snow Depth (m)	0.073	0.032	0.010	0.190
Surface Elevation (m ASL)	0.127	0.032	0.070	0.265
S/I Interface (m ASL)	0.054	0.028	-0.065	0.197
EM Ice Thickness (m)	0.477	0.035	0.376	0.592
*Measured Ice Thick (m)	0.565	0.067	0.470	0.690
*Measured Freeboard (m)	0.037	0.035	0.010	0.110

211 *Note: measured ice thickness and freeboard values are limited (< n)

212 In heavily deformed areas of Belgica Station containing thick snow cover, interface
 213 flooding was observed to be common. Level surveys performed along two 300 meter transect
 214 lines over a 3 week period at the Fabra Site indicated that the snow/ice interface initially
 215 contained approximately 63% flooded snow cover (in profile) at the beginning of October.
 216 During the three week period, the percentage of interface flooding along these transect profiles
 217 increased to as much as 78%. These findings were verified by excavation of numerous snow pits
 218 along the two transect lines. In particular, an experiment using temperature “button” dataloggers
 219 in Snow Pit 2G captured an initially flooded snow interface that was subsequently flooded to a
 220 higher level in the snow pack during a storm event between October 17 and 19, 2007. The time
 221 series of temperature in the snow pack and slush layer, given in *Figure 7*, shows that temperature

222 increased during the warming trend of the storm event. The data logger in the snow pack +30 cm
223 above the original flooded interface decreased post-storm in response to lower air temperature,
224 however, at the +20 cm level above the original flooded interface the temperature remains
225 relatively constant near the freezing point of sea water, thus indicating the snow pack was
226 flooded to this level. Snow Pit 2G was subsequently excavated at the conclusion of the
227 experiment on October 22 and the presence of an additional 25 cm of flooded snow cover was
228 confirmed by direct measurement. The interpretation of flooding events using the time series of
229 temperature in profile through the snow pack, as illustrated in the Snow Pit 2G experiment, is
230 consistent with previous interpretation of flooding events from IMB buoy data of the
231 SOGLOBEC experiment (Figure 2).

232 The IMB buoy temperature profiles from SIMBA were obtained from thermister string
233 data at the Brussels and Liege Sites. In the case of the Brussels Site, two IMB buoys were
234 present in locations where no flooding of the snow/ice interface was observed. The temperature
235 time series corresponding to the original snow/ice interface at the time of buoy deployment was
236 used for comparison with AMSR-E values for this location, as shown in *Figure 8*. Due to the
237 thinner snow cover and absence of interface flooding, these sea ice interface temperature records
238 are considered to represent the low range of temperature values (colder) for the specific snow
239 and ice conditions present across Belgica Station. In general, the AMSR-E ice temperature is still
240 considerably lower than the in situ ice temperatures, except in the time interval between October
241 8 and October 16. On both sides of this time interval, the AMSR-E ice temperature appears to
242 correlate approximately with the IMB buoy records, but at lower temperature values. During the
243 time interval from October 8 to 16, the AMSR-E ice temperature has no apparent correlation

244 with in situ temperature and the AMSR-E ice concentration (Figure 7) dips to concentrations
245 below 95%.

246 In the cases where interface flooding was observed (ie. Liege Site, Fabra Site),
247 temperatures from the sea ice interface were interpreted from the profile of thermister data. The
248 sea ice temperature in these areas is anticipated to represent the high range of temperature values
249 (warmer) due to the presence of unfrozen sea water at the interface and deep snow cover that
250 provides insulation from lower air temperatures. The ice interface temperature for flooded areas
251 typically falls narrowly within a range from -1.8 to -2.0 °C. A plot of the ice interface
252 temperature for the Liege IMB is given in *Figure 9*.

253 **4. Discussion on the difference between AMSE-E Sea Ice Temperature and in situ** 254 **measurements**

255 It is difficult to compare in situ sea ice temperature with AMSR-E ice temperature due to
256 significant differences in scale and the variability of snow and ice conditions within the coarse
257 resolution of an AMSR-E pixel. It is therefore necessary on some level to make a qualitative
258 assessment based on observed characteristics of the snow and ice cover and to evaluate in situ
259 “point” data in terms of representative site conditions. Although SOGLOBEC temperature data
260 shows no correlation with AMSR-E ice temperature, the point information may or may not
261 necessarily represent spatial variability within a single AMSR-E pixel of the Marguerite Bay
262 area. This region reported by Perovich (2004) to have approximately 20% area with flooded
263 snow/ice interface around the time of buoy installation. In situ ice temperatures from the IMB
264 buoy indicated the ice floe was not initially flooded but affected by a series of flooding and re-
265 freezing events that occurred weeks and months after installation. Assuming the IMB buoy
266 represents typical “intermediate” ice conditions for the area, the AMSR-E product does not

267 appear to perform with any reasonable degree of accuracy. In Figure 2, following the first week
268 of IMB buoy operation, the snow and ice temperature rises in response to rising air temperatures,
269 however the AMSR-E ice temperature decreases dramatically during the same period.

270 Areas from Belgica Station with extensive surface flooding (ie. Fabra Site) show the
271 interface temperature strongly influenced by thick snow cover providing thermal insulation from
272 colder air temps and presence of warm sea water in flooded areas. Where refreezing occurs, ice
273 temperatures will be lower but still limited by thermal insulation of thick snow cover. This
274 results in a narrow range of ice interface temperatures for flooded areas that fluctuate around -2°
275 C. The AMSR-E ice temperature is generally 6 to 12 degrees colder over the record at the Fabra
276 or Liege Sites.

277 Areas of level, thinner first year ice with thin snow cover (ie. Brussels site) represent the
278 colder spectrum of ice conditions present at Belgica Station. The plot given in *Figure 10* shows
279 very poor to no correlation of AMSR-E and in situ ice temperature for both IMB buoys during
280 the drift period of Belgica station. The low ice concentration (<99%) represented in the data set
281 between October 8 and 16, 2007 was removed as shown in *Figure 11*. The scatterplot shows a
282 somewhat better correlation, but still poor. The AMSR-E ice temperatures are generally much
283 lower than in situ temperatures representing even the cold end of the spectrum of ice conditions,
284 and therefore, considering the mixture of ice types represented by a single AMSR-E pixel, fall
285 outside the range of expected values.

286 **5. Conclusion remarks**

287 1) In situ data shows that snow/ice interface flooding has a significant effect upon ice
288 temperature. Where a flooded sea ice interface exists, typically have much deeper snow pack,
289 increased roughness, and warmer in situ sea ice temperatures. Based on ASPeCt observations

290 and snow pit data collected, Belgica Station is characterized as a composition of approximately
291 40% thick multi-year ice with deep snow cover and 60% thick first year ice with thinner snow
292 cover. The Brussels Site contains thinner first year ice and thin snow cover and therefore
293 represents the cold end member of the major ice types present. The Fabra Site represents the
294 warmer end member due to highly deformed surface, thick snow cover, and extensive snow/ice
295 interface flooding.

296 2) The AMSR-E ice temperature product contains a mixture of information in each pixel
297 regarding spatial variation of ice type and snow conditions. The AMSR-E ice temperature shows
298 no correlation with either flooded areas or other ice types evaluated and was generally much
299 lower than even coldest ice conditions at Belgica Station. The AMSR-E ice temperature, for the
300 most part, falls outside the range of measured in situ values and is not representative of in situ
301 temperatures from a spatial mixture of ice types and snow conditions

302 3) Ice concentration significantly affects the AMSR-E ice temperature product. Lower ice
303 concentration appears to negatively influence the algorithm performance. For SOGLOBEC data,
304 the end of the record shows erratic fluctuations in AMSR-E ice temperature which corresponds
305 with lower ice concentration. Using data from the Brussels Site, removing ice concentration
306 below 99% yield a better correlation with AMSR-E, but still not good. There are differences
307 between ABA and NT2 (Parkinson and Comiso, 2008). Existing AMSR-E ice temperature
308 algorithm initially uses a reference emissivity for each pixel that carries a mixture of information
309 based on an initial concentration derived from open water and pure ice tie points. The physical
310 temperature (believed to be the sea ice interface) is subsequently calculated using 6.9 GHz
311 brightness temperature and the ice concentration is subsequently recomputed using different

312 channels. Further study is needed to evaluate the effects of ice concentration on the algorithm,
313 including a means to verify ice concentration independent of passive microwave methods.

314 4) Further study is warranted to both evaluate the AMSR-E ice temperature product and
315 to provide algorithm enhancements to improve performance. Sea ice temperature is an important
316 parameter needed to understand sea ice and climate. Due to the physical constraints related to in
317 situ measurements, remote sensing of sea ice temperature on a circumpolar basis is necessary for
318 long term monitoring and to provide input to climate and ocean models to assess and predict
319 change.

320 5)

321 **Acknowledgments:** Supported by NSF Grant ANT 0703682- Sea Ice Mass Balance in the
322 Antarctic to UTSA (PI S.F. Ackley), M.J. Lewis acknowledges the support of Southwest
323 Research Institute. The authors wish to thank Don Perovich for SOGLOBEC data, Blake
324 Weissling for his assistance with ArcInfo data processing, and the crew and support personnel
325 from the NB Palmer.

326

327 **References**

328 Andersen et al, 2006

329 Brabant, F. 2008

330 Comiso, et al 2003

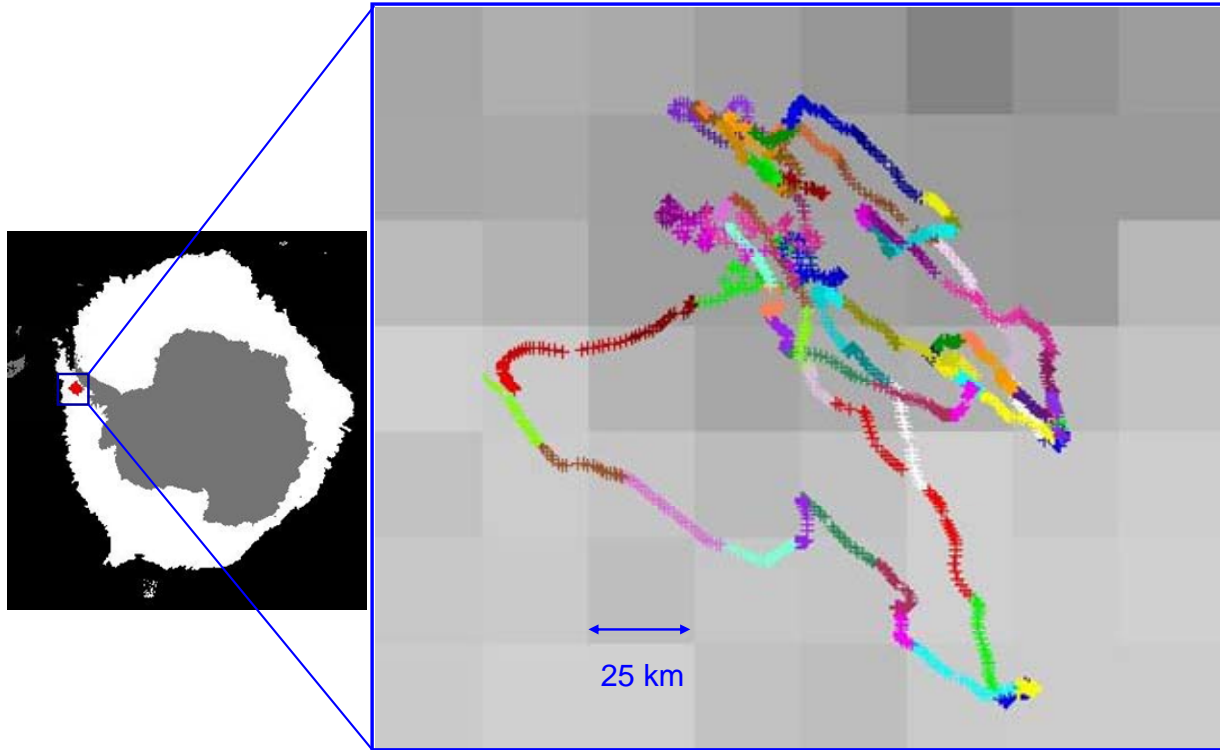
331 Comiso et al 2008

332 De Lille, B. 2008

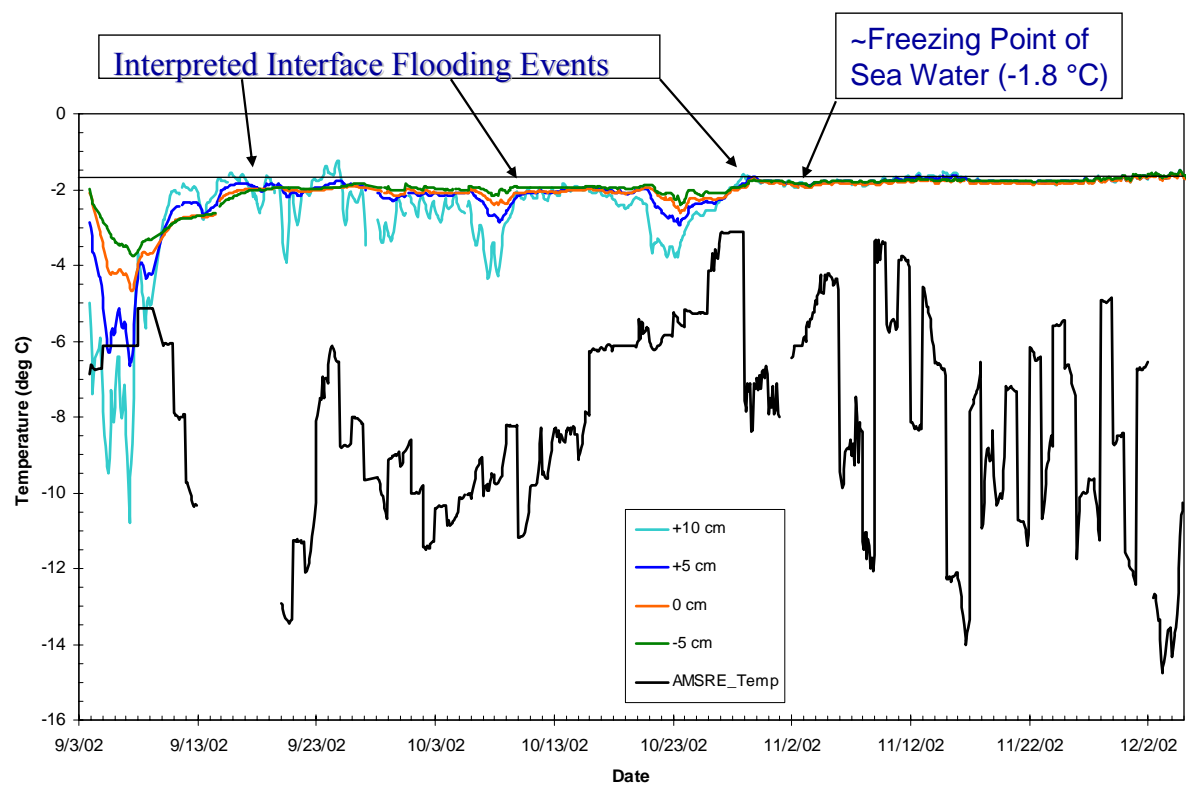
333 Ackley et al 2006

- 334 Golden, K. (2001) Brine percolation and the transport properties of sea ice, *Annals of*
335 *Glaciology*, 33, 28-35.
- 336 IGOS, 2007
- 337 Lewis and Xie, 2006
- 338 Lewis et al. 2006
- 339 Parkinson 2004
- 340 Parkinson and Comiso, 2008
- 341 Perovich D.K., 2004
- 342 Weeks, W.F. and S.F. Ackley (1986), The Growth Structure and Properties of Sea Ice, in *The*
343 *Geophysics of Sea Ice*, N. Untersteiner, ed., Nato ASI Series, Physics, Vol. 146, Plenum
344 Press.
- 345 Worby and Allison, 1999

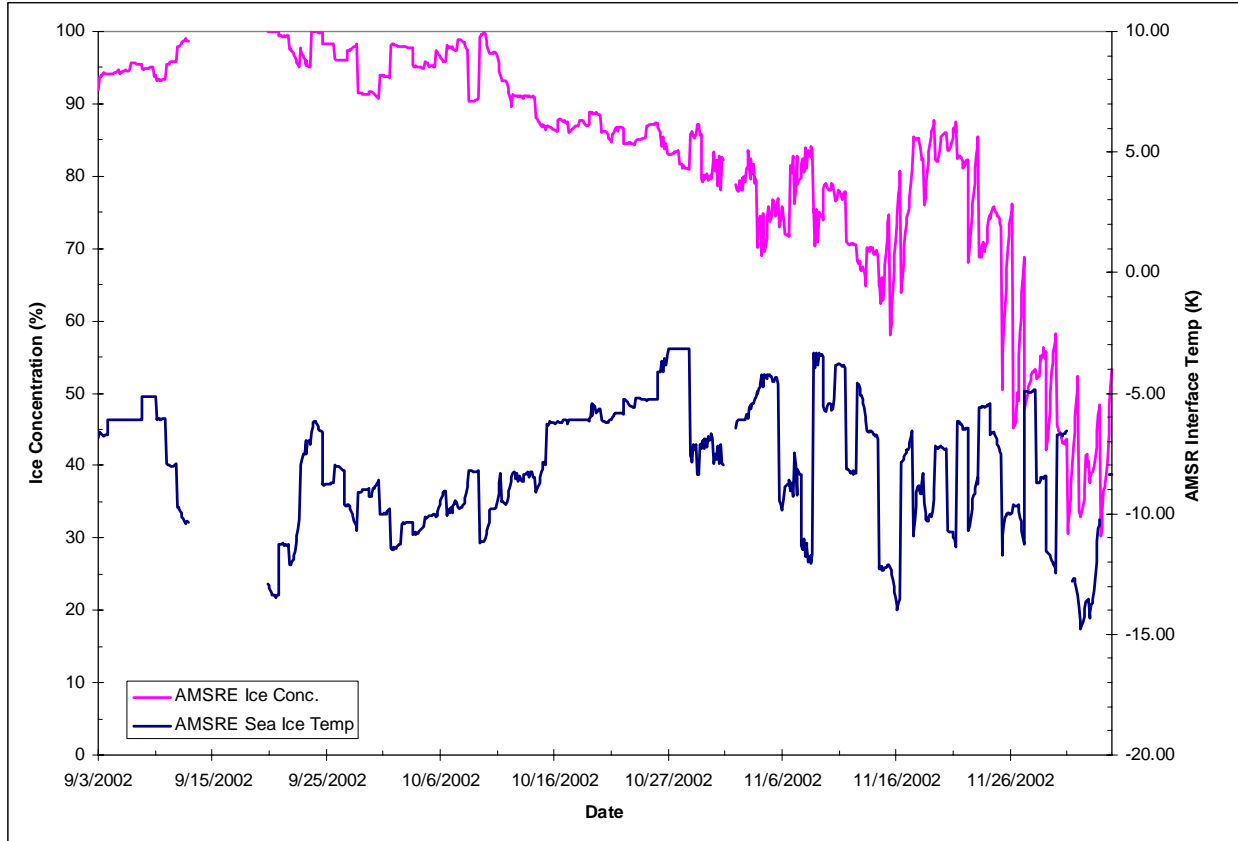
346



347
348 Figure 1.



349
 350
 351 Figure 2



352
353
354

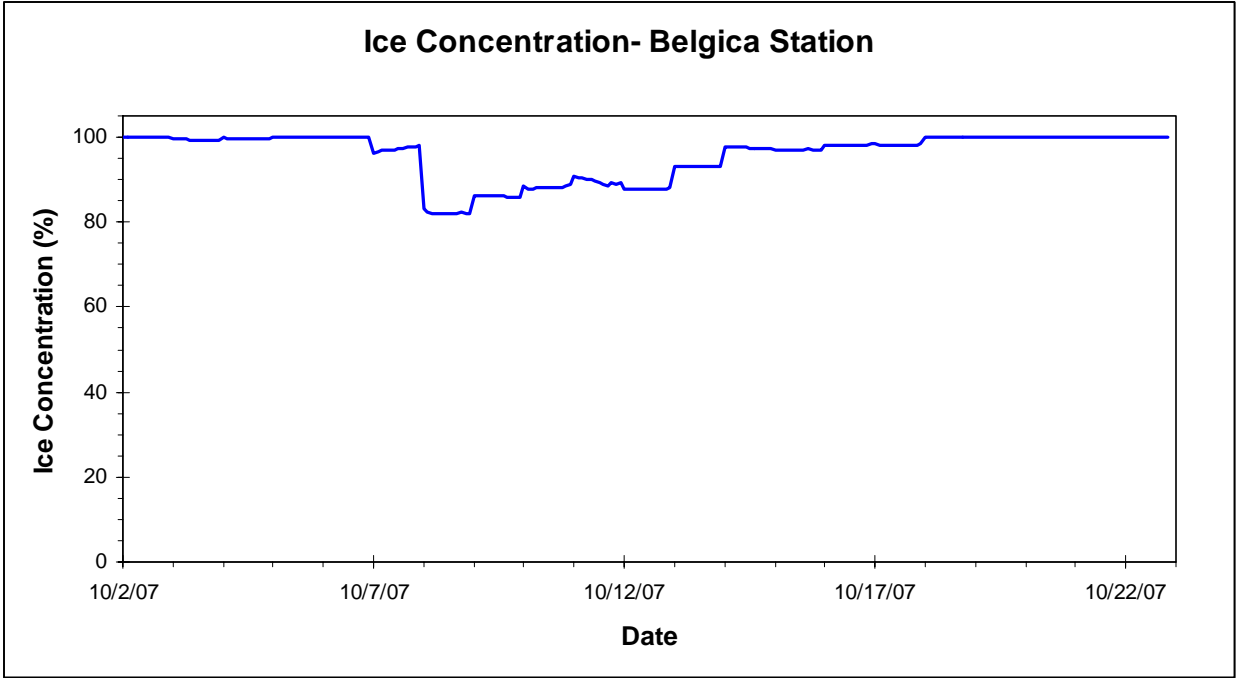
Figure 3



Brussels
Site

355
356
357

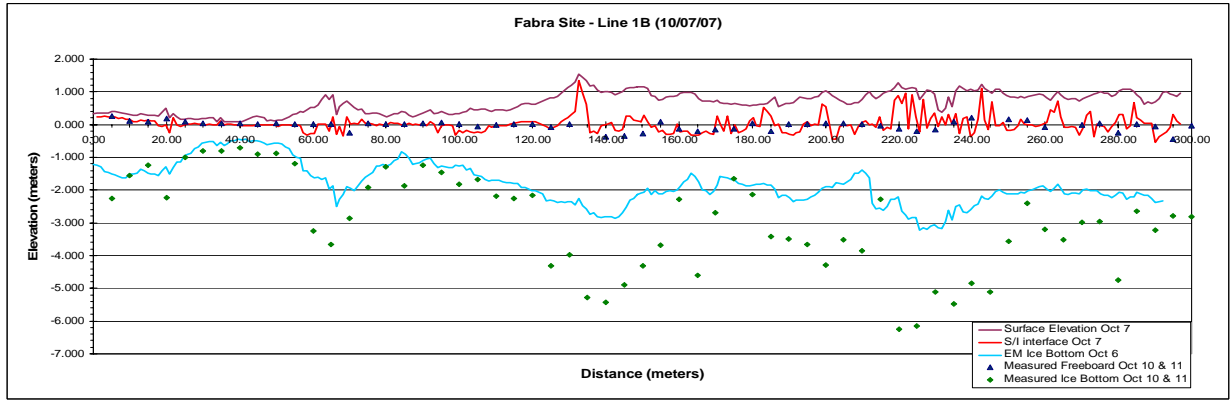
Figure 4



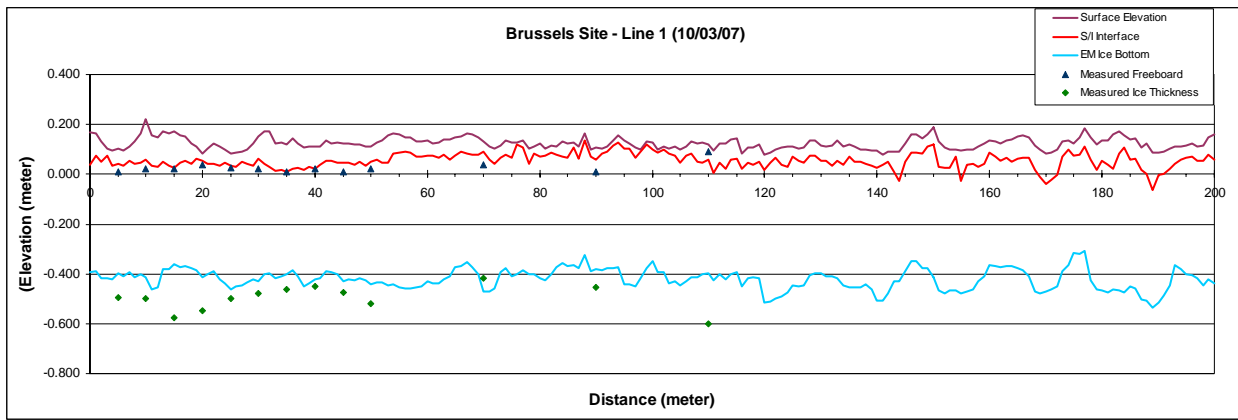
358
359
360

Figure 5

361

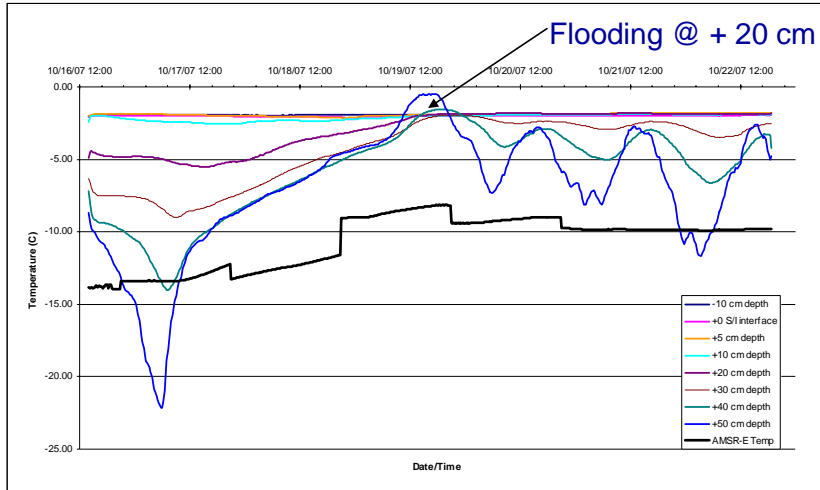


362
363



364
365
366

Figure 6 a) Fabra Site, b) Brussels Site

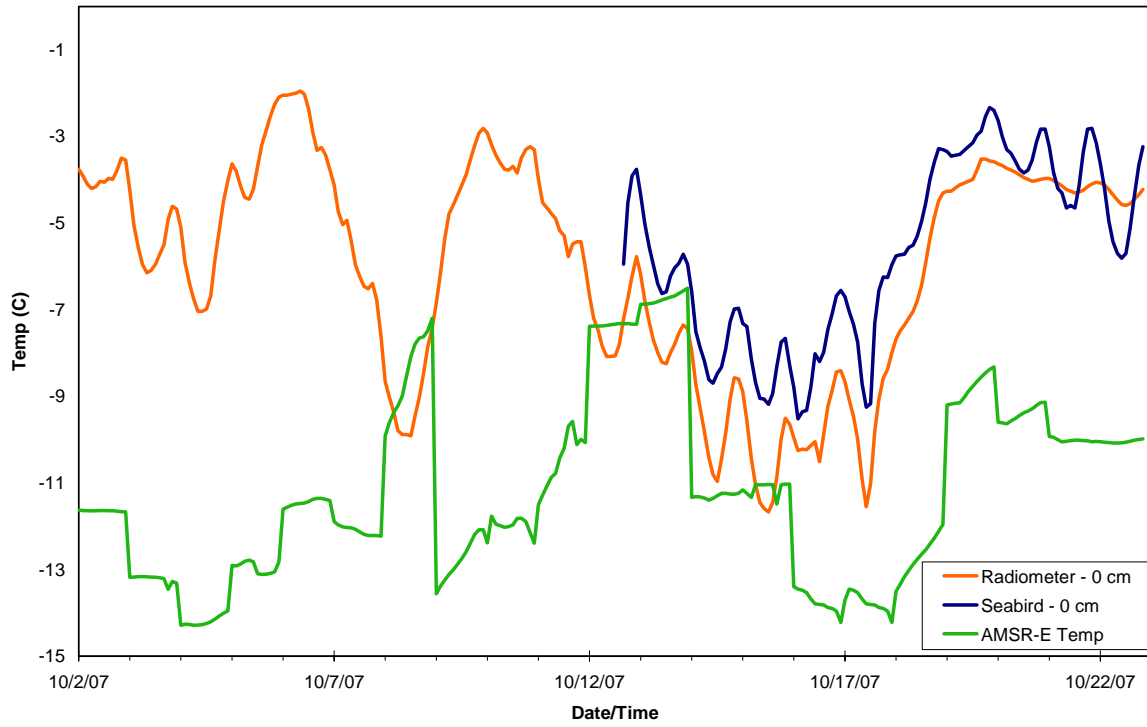


368
369

Figure 7 (or add a snowpit profile graphic here instead of photos)

370

Brussels Site (SIMBA) IMB Temperatures

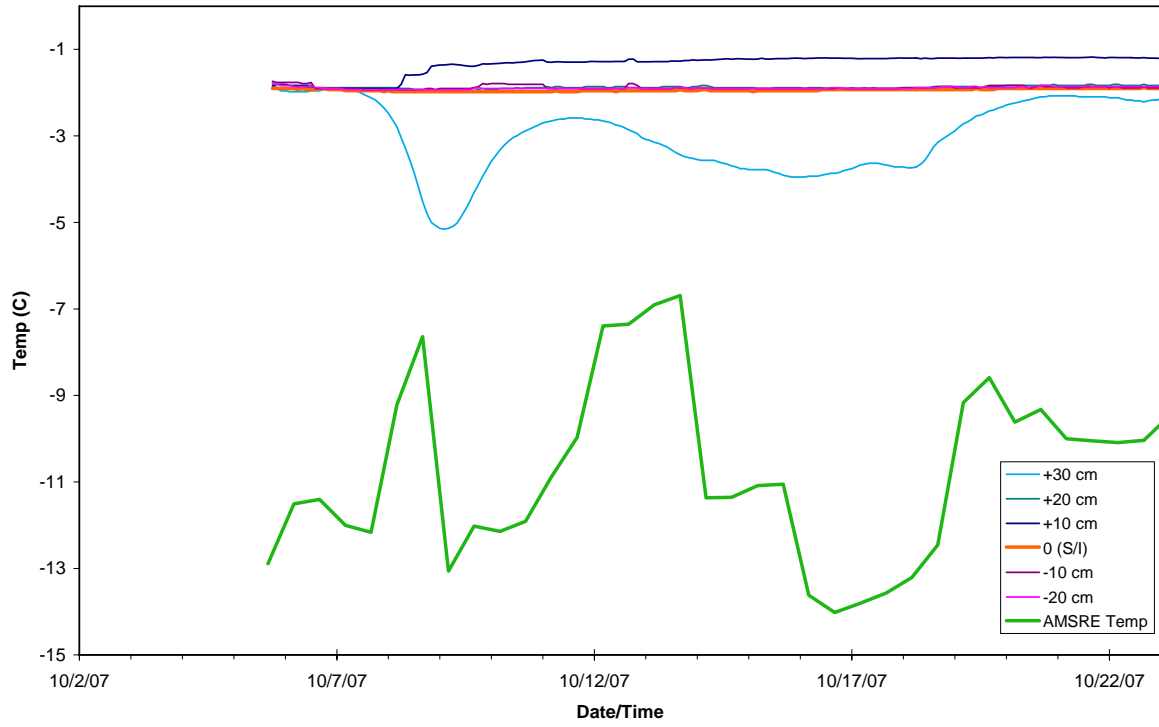


371

372

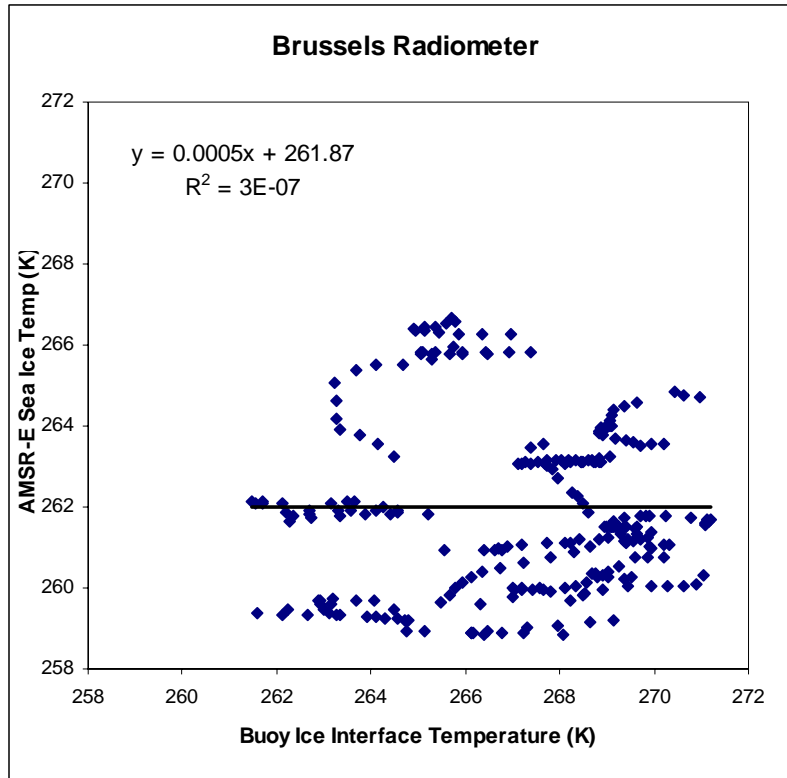
373 Figure 8

Liege Site (SIMBA) IMB Temperatures

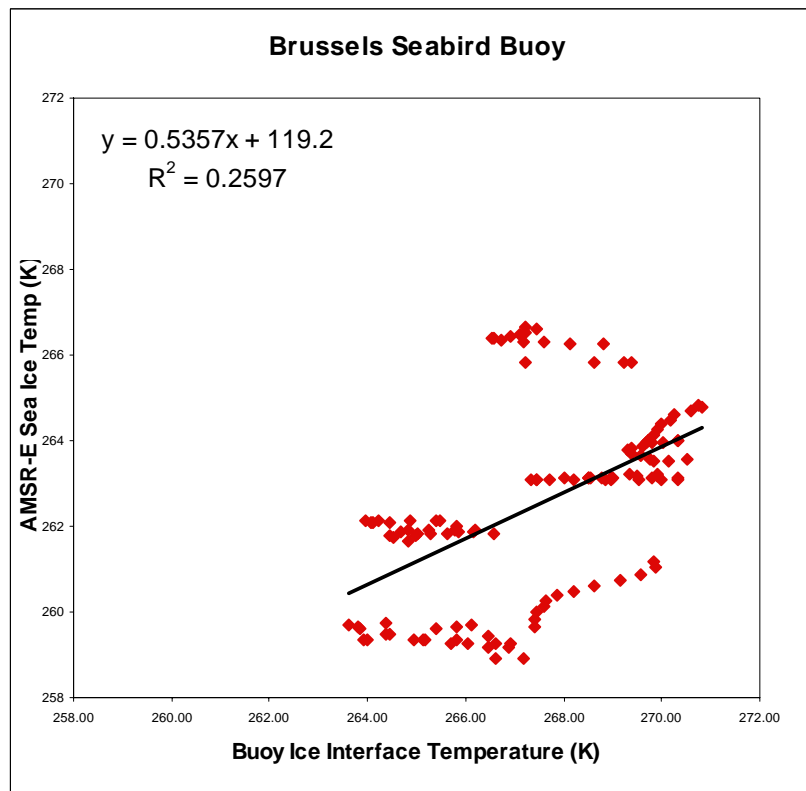


374
375 Figure 9

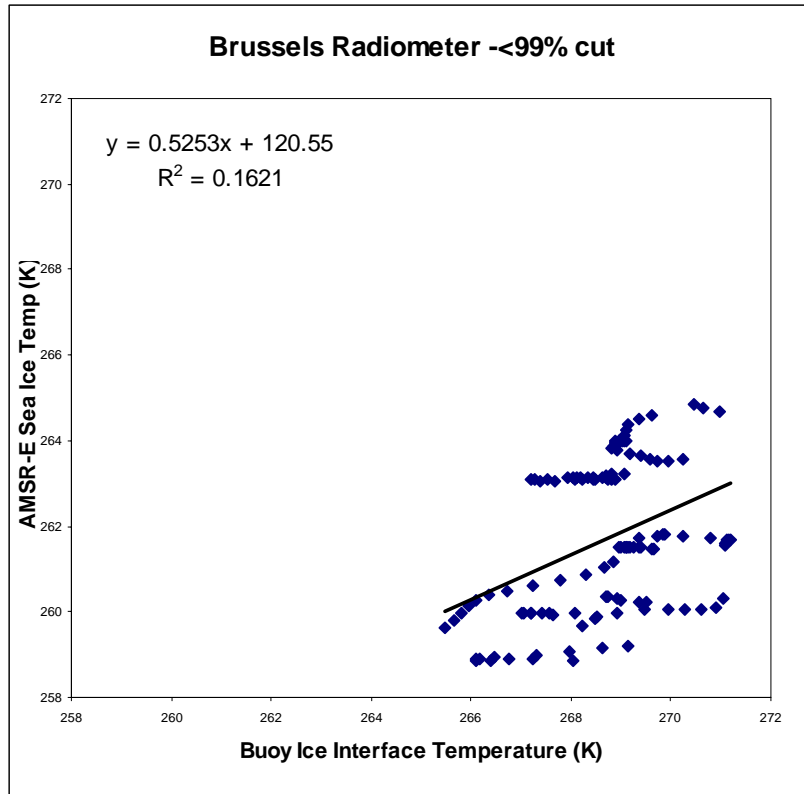
376
377



378
379
380

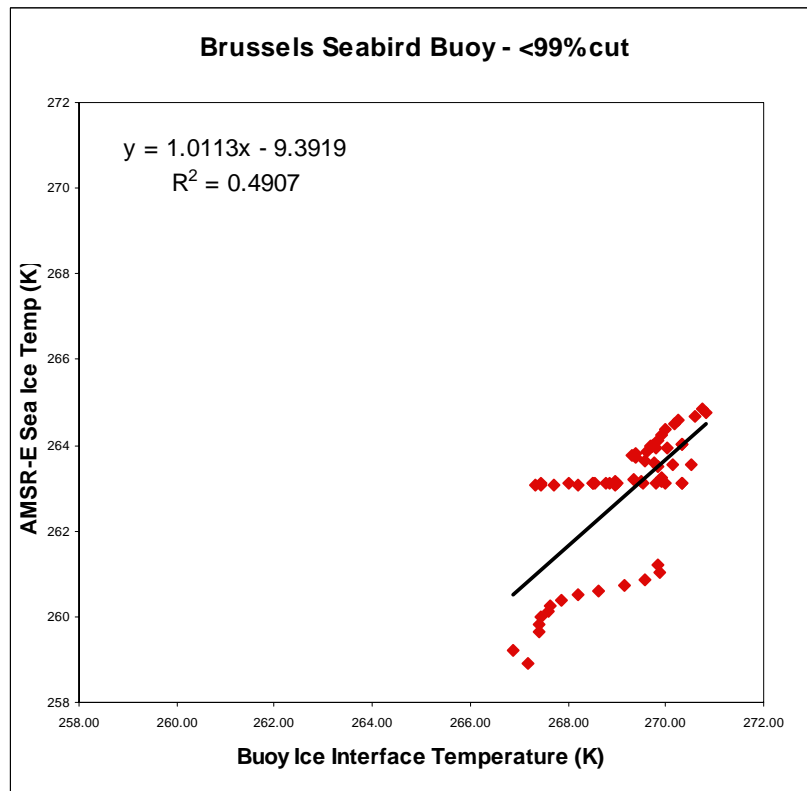


Similar comments as the above. You seem have 5 groups?
Figure 10



381
382

Two groups?



383
384

Figure 11 three groups?